Solution Structures of 5-Fluorouracil-Substituted RNA Duplexes Containing G-U Wobble Base Pairs†

Parag V. Sahasrabudhe and William H. Gmeiner*

Eppley Institute for Cancer Research and Department of Pharmaceutical Sciences, University of Nebraska Medical Center, Omaha, Nebraska 68198-6805

Received January 10, 1997; Revised Manuscript Received March 19, 1997⊗

ABSTRACT: The structures and stabilities of three RNA duplexes that differed only in the position of 5-fluorouridine (FUrd) substitution were elucidated using NMR spectroscopy and UV hyperchromicity studies to determine if FUrd substitution altered the structure or stability of RNA duplexes that contained G-U base pairs. The duplexes investigated corresponded to the region of the U4−U6 snRNA complex that contained the 5′ terminus of U4 snRNA. The control duplex contained a G-U wobble base pair and also a G-A mismatched base pair. FUrd was substituted in one duplex at the G-U wobble base pair and in the second duplex at an A-U base pair adjacent to the wobble base pair. FUrd substitution slightly destabilized the duplex that contained a G-FU base pair but stabilized the duplex that contained an A-FU base pair. NOESY spectra were used to determine interproton distances, and these distance constraints were used in a restrained molecular dynamics protocol to determine the three-dimensional structures of these RNA duplexes. Analyses of helical parameters, backbone torsion angles, and rms deviations between the final structures revealed no systematic differences due to FUrd substitution in RNA duplexes that contained G-U base pairs. The G-FU base pair adopted wobble geometry, while the G-A mismatch formed a sheared base pair. NOESY spectra in H_2O solution revealed the imino ^1H from FUrd exchanged more rapidly with solvent than did the Urd imino ^1H but did not show the G-FU base pair adopted an ionized structure. Reduced stacking occurred for the G-FU base pair relative to the G-U base pair in the time-averaged structure, and this, rather than ionization of the base pair, was responsible for the slight destabilization of the duplex that contained the G-FU base pair.

5-Fluorouracil (FUra)[1] is an antineoplastic agent used singly or in combination with folate analogs such as leucovorin and methotrexate, as well as others drugs, for the treatment of solid tumors in humans (Pratt *et al*., 1994). FUra is converted intracellularly to FdUMP, a dUMP analog that together with reduced folate and thymidylate synthase (TS) forms a stable ternary complex that irreversibly inhibits TS enzymatic activity (Santi *et al*., 1974). Exposure of cells in culture to FUra results in a cytostatic condition referred to as "thymineless cell death" (Weckbecker, 1991; Houghton *et al*., 1994). Simultaneous exposure of cells in culture to both FUra and dTMP also results in cytostasis, implicating non-TS inhibitory processes in the growth inhibitory activity of FUra (Spiegelman *et al*., 1980). The cytostatic activity of FUra due to mechanisms other than TS inhibition is not well understood; however, metabolic activation of FUra to FdUTP and FUTP occurs readily and is followed by their incorporation into nucleic acids (Tanaka *et al*., 1981; Chaudhuri *et al*., 1958). FdUTP is cleaved by dUTPase (Daher *et al*., 1990) and, when incorporated into DNA, is removed by uracil deglycosylase (Ingraham *et al*., 1980). Significant incorporation of FdUTP into DNA occurs only after dTMP levels are depleted following TS inhibition and result in strand breaks (Schuetz *et al*., 1986; Cheng & Nakayama, 1983). FUTP is readily incorporated into cellular RNA, and no repair processes that remove 5-fluorouridine (FUrd) from RNA are known. FUrd incorporation into both pre-mRNA and snRNA has been shown to reduce the efficiency of pre-mRNA splicing (Parker & Cheng, 1990; Schmittgen *et al*., 1994; Doong & Dolnick, 1988). Similarly, Urd → FUrd substitution in pre-rRNA reduced the efficiency of rRNA assembly (Wilkinson & Pitot, 1973).

The physicochemical basis for alteration of RNA structure and function as a consequence of Urd → FUrd substitution is not known. FdUrd incorporation has been shown to affect the structures of duplex DNA near the site of substitution (Stolarski *et al*., 1992). Specifically, substitution of FdUrd in duplex DNA increased the roll angle at the base steps involving FdUrd and increased the curvature of the DNA duplex. In contrast, site-specific FUrd substitutions in duplex RNA increased the rmsd for the base pairs directly substituted with FUrd but did not affect the curvature of duplex RNA (Sahasrabudhe *et al*., 1996). FUrd substitution also increased the stability of RNA duplexes consisting of only Watson−Crick base pairs (Sahasrabudhe *et al*., 1995; Gmeiner *et al*., 1994a). RNA frequently adopts secondary structures rarely observed for DNA, including noncanonical base pairs, single- and multiple-base bulges, and internal loops (Saenger, 1984). The effects of FUrd substitution at or near base pair

† This research was supported by funds from NIH-NCI R29CA60612 (W.H.G.) and NIH-NCI CA-36727.

* Address correspondence to this author. Phone: (402) 559-4257. Fax: (402) 559-4651. E-mail: bgmeiner@unmc.edu.

⊗ Abstract published in *Advance ACS Abstracts,* May 1, 1997.

[1] Abbreviations: FUra, 5-fluorouracil; FUrd, 5-fluorouridine; FdU, 5-fluoro-2′-deoxyuridine; FdUMP, 5-fluoro-2′-deoxyuridine monophosphate; FdUTP, 5-fluoro-2′-deoxyuridine triphosphate; FUTP, 5-fluorouridine triphosphate; dTMP, 2′-deoxythymidine triphosphate; TS, thymidylate synthase; G-U, guanosine-uridine; dG-FdU, 2′-deoxyguanosine-2′-deoxy-5-fluorouridine; G-FU, guanosine-5-fluoro-uridine; A-U, adenosine-uridine; A-FU, adenosine-5-fluorouridine; rMD, restrained molecular dynamics; rmsd, root mean square deviation.

S0006-2960(97)00057-3 CCC: $14.00

mismatches or G-U wobble base pairs could be more significant toward its biological effects than FUrd substitution in A-U base pairs. No high-resolution structures of RNA duplexes containing noncanonical base pairs involving FUrd have been previously reported, although NMR and X-ray studies of duplex DNA containing a dG-FdU base pair and the structure of *Escherichia coli* $tRNA^{Val}$ containing G-FU wobble base pairs were reported (Sowers *et al*., 1988; Coll *et al*., 1989; Chu & Horowitz, 1989).

The stem II duplex of the U4−U6 snRNA complex from *Saccharomyces cerevisiae* has been shown to be exquisitely sensitive to single nucleotide mutations. In fact, the U6C mutation that converts an A-U base pair in stem II into an A-C mismatched base pair was lethal to this strain of yeast (Hu *et al*., 1995). Conditional growth resulted from several other single nucleotide substitutions in this region. While the effects of Urd → FUrd substitution may be expected to be less deleterious than Urd → Cyt substitution, little is known about mismatched and wobble base pair structure and stability in RNA substituted with FUrd. In order to gain greater insight into the effects of FUrd on the structure and stability of the stem II duplex from the U4−U6 snRNA complex, we have prepared synthetic oligoribonucleotides with site-specific substitution of FUrd (Gmeiner *et al*., 1994b). The stabilities of these RNA duplexes were investigated using UV hyperchromicity studies. The three-dimensional structures of these RNA duplexes were determined using NMR spectroscopy in conjunction with complete relaxation matrix analysis and restrained molecular dynamics simulations. These investigations conclusively showed that Urd → FUrd substitutions did not systematically affect the structures of RNA duplexes that contained mismatched and wobble base pairs. These studies provide a model for the association of U4 and U6 snRNAs via formation of the stem II duplex *in vivo*. This model suggests that the unique structural and thermodynamic stability properties of this duplex arise from formation of mismatched and wobble base pairs but that the substitution of uridine by 5-fluorouridine in this sequence context is not a major determinant in the RNA-mediated effects of 5-FU.

EXPERIMENTAL PROCEDURES

Solid-Phase Synthesis of Oligoribonucleotides. The synthesis and purification of 5′-*O*-(4,4′-dimethoxytrityl)-2′-*O*-(*tert*-butyldimethylsilyl)-5-fluorouridine 3′-(cyanoethyl *N*,*N*′-diisopropylphosphoramidite) and purification of RNA containing FUrd were done as previously described (Gmeiner *et al*., 1994b). Syntheses were performed using an Applied Biosystems 380B DNA synthesizer at the 10 μmol scale. The material was purified on a denaturing 20% polyacrylamide gel. Three 8mer RNA duplexes were prepared that differed only in the location of FUrd substitution. The sequence selected corresponds to the "A" half of the stem II sequence from the U4−U6 snRNA complex that included the 5′ terminus of U4 snRNA (Figure 1). This sequence contained an A-G mismatched base pair and a G-U wobble base pair. The control sequence is denoted S2A-C throughout the text, while the sequence containing a G-FU base pair is denoted S2A-GF and the sequence containing an A-FU base pair S2A-AF (Figure 1).

Thermodynamic Analyses. Thermodynamic analyses for the FUrd-substituted and control duplexes were made as previously described (Sahasrabudhe *et al*., 1995). Six measurements were made for each sample. Melting curves for the three 8mer duplexes were acquired at 12 different concentrations from 10^{-4} to 10^{-6} M in a buffer consisting of 0.1 M NaCl and 2 mM sodium cacodylate at pH 7.3. All the initial and final absorbance values were between 0.25 and 2.2 (optical density). Six measurements were made for each sample at each concentration. Numerical values for the thermodynamic parameters $\Delta G°$, $\Delta H°$, and $\Delta S°$ associated with the duplex to single-stranded transition for each of the RNA duplexes were obtained using the software written by Petersheim and Turner (1983). Values of χ^2 resulting from the parametric fitting for each of the experimental melting curves were less than 10^{-5}. Melting temperatures, T_m, were calculated from the first derivative of the absorbance versus temperature data for each duplex at each concentration. Numerical values for $\Delta H°$ and $\Delta S°$ were obtained from plots of $1/T_m$ versus $\log(c_T/4)$ (Borer *et al*., 1974).

NMR Spectroscopy. Samples for NMR analysis were prepared by mixing equimolar amounts of the two strands. Each sample contained about 50 absorbance units of one duplex in 0.6 mL of 2 mM sodium cacodylate (pH 7.3), 100 mM NaCl, and 0.2 mM disodium EDTA. All NMR experiments were performed using a Varian UNITY 500 NMR spectrometer with a 3 mm [^{1}H,^{13}C,^{31}P] triple-resonance *z*-gradient probe except ^{19}F spectra that were acquired using a Nalorac ^{1}H−^{19}F dual high-band probe. ^{1}H spectra were referenced to internal TSP (0.00 ppm), and ^{19}F spectra were referenced to external α,α,α-trifluorotoluene (0.00 ppm). One-dimensional NOE spectra in H_2O were obtained at 15 °C using a 1−3−3−1 binomial pulse for water suppression (Hore, 1983). Two-dimensional NOESY spectra in ^2H_2O were acquired for three different mixing times, 100, 150, and 200 ms, using standard three-pulse sequences with States's method of phase cycling (States *et al*., 1982). Two hundred fifty-six free induction decays (FIDs), 16 scans each, were collected in the t_1 dimension with alternating block acquisition. Two thousand data points were collected over a spectral window of 5000 Hz in the t_2 dimension. A relaxation delay of 10 s between scans was used to allow nearly complete relaxation of magnetization. All data were processed using VNMR v. 5.1 from Varian. The data were extended using forward linear prediction in the t_1 dimension, to create the final matrix containing 2K × 2K points (Babcook *et al*., 1996). Baseline correction was applied to both dimensions after the second Fourier transform.

Calculation of Interproton Distances. Interproton distances were calculated from NOESY cross-peak intensities using MARDIGRAS (Borgias & James, 1989, 1990). A complete relaxation matrix was created for each duplex using experimental intensities, and estimated intensities from the geometry of the starting structure for those cross-peak intensities which were unavailable from the experimental data. The diagonal and off-diagonal terms were compared iteratively until the sum of the residual errors was minimized. Calculations for each duplex were carried out with three experimental data sets (100, 150, and 200 ms mixing times), two geometries for the initial structure (A-form and B-form double helix), and three values for the isotropic correlation times (1.5, 2.0, and 2.5 ns). Eighteen calculations were carried out for each duplex, yielding 18 sets of interproton distances. These data sets were averaged, and the calculated

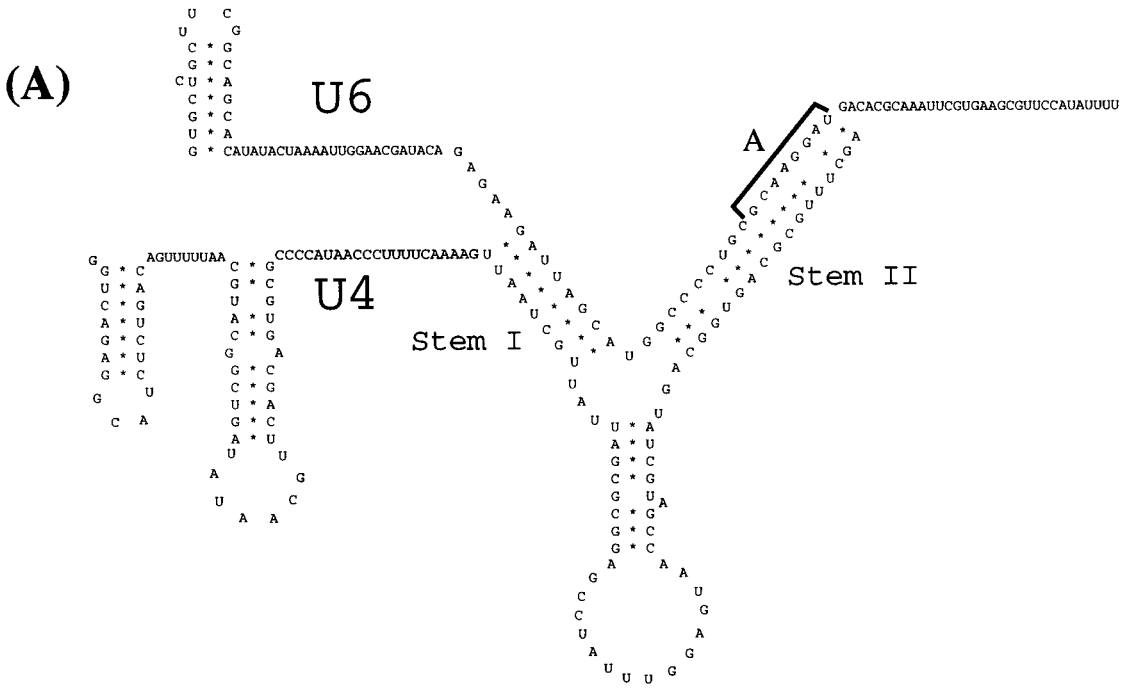

(B)

Sequences from the stem II of U4-U6 snRNA complex used in this study:

		1	2	3	4	5	6	7	8
S2A-C:	5'-	A	G	C	U	U	U	G	C
	3'-	U	A	G	G	A	A	C	G
		16	15	14	13	12	11	10	9
S2A-GF:	5'-	A	G	C	F	U	U	G	C
	3'-	U	A	G	G	A	A	C	G
S2A-AF:	5'-	A	G	C	U	F	U	G	C
	3'-	U	A	G	G	A	A	C	G

FIGURE 1: (A) Structure of the human U4−U6 snRNA complex. The bracketed (A) region of stem II contains the sequence that was considered in the present study. (B) The sequences of the three duplex oligoribonucleotides studied. S2A-C is the native sequence, while S2A-GF contains FUrd substitution at the G-U base pair and S2A-AF FUrd substitution at the A-U base pair indicated.

standard deviation was used to set the width of the flat part of the potential well for distance constraints in the restrained molecular dynamics calculations.

Construction of Molecular Models. Initial structures for each duplex were constructed with A-form (Arnott & Hukins, 1972) and B-form (Arnott & Hukins, 1973) double-helical geometry using SYBYL. Coordinate and topology files were created using AMBER 4.1 (Pearlman *et al*., 1995). The modified 5-fluorouridine nucleosides were created using bond angles and bond lengths from a previously published crystal structure (Harris & McIntyre, 1964). Large hexahydrated sodium ions with a 5 Å radius (Singh *et al*., 1985) were added to mimic counterion effects. These counterions were placed along the phosphate bisection, 6 Å away from the phosphorus, and were free to move during energy minimization and molecular dynamics procedures. The starting structures were energy minimized *in vacuo* using a combination of steepest descent and conjugate gradient methods using AMBER 4.1.

Restrained Molecular Dynamics. Restrained molecular dynamics calculations were carried out *in vacuo* using the SANDER module of AMBER 4.1. Distance and angular constraints were included in the force field as pseudoenergy terms, which had the form of a flat well with parabolic sides extending 0.5 Å or 5° from the flat part of the potential well and continued linearly beyond these margins (Stolarski *et al*., 1992). The MARDIGRAS calculations determined the width of the flat portion of the potential well. The backbone dihedral angles were constrained in a broad allowed region of the torsional angle space to preserve the right-handed character of the RNA helix during the molecular dynamics simulations (Baleja *et al*., 1990; Gronenborn & Clore, 1989; Suzuki *et al*., 1986). Additional distance and angular constraints were added between the bases to maintain Watson−Crick geometry during the rMD simulations (Schmitz *et al*., 1992). Flat angles were determined by the three atoms that formed the hydrogen bond. Constraints representing hydrogen bonds were not added for the G-A mismatched

Table 1: Thermodynamic Parameters for the RNA Duplexes Considered in This Study

	average fitted parameters[a]			
duplex	$\Delta H°$ (kcal/mol)	$\Delta S°$ (cal mol^{-1} °C^{-1})	$\Delta G°_{37}$ (kcal/mol)	T_m (°C)
S2A-C	-37.8 ± 1.6	-105.3 ± 5.2	-5.1 ± 0.01	30.5 ± 0.2
S2A-GF	-32.5 ± 0.3	-88.8 ± 0.8	-4.9 ± 0.01	28.5 ± 0.1
S2A-AF	-44.7 ± 0.9	-127.1 ± 2.9	-5.2 ± 0.02	32.3 ± 0.1

[a] The data were analyzed using a Student's *t* test; $P < 0.002$.

base pair. The only additional constraint added for the G-A base pair was between the C1′ atoms of the bases, which was broader (10.5−12.0 Å) compared to the same constraint for other base pairs. An average of 298 constraints were used in the rMD simulations for each duplex with 161 of these based on NMR spectroscopic data (Table 4). The rMD simulations were carried out for 30 ps with 1 fs steps. All atoms within a 35 Å radius were included in nonbonded interactions. SHAKE was used to constrain all bonds (Ryckaert *et al*., 1977), and translational and rotational motions were removed every 100 steps. Application of the NMR constraints and the duration of the rMD simulations were done as previously described (Mujeeb *et al*., 1993).

The structures obtained from rMD simulations for each initial geometry (final A-form and final B-form) resulted from averaging the coordinates for the three structures obtained with different seed values for initial velocities. The final structure for each duplex was obtained by averaging the two penultimate structures (final A-form and final B-form) for a particular duplex. The final structure was subsequently subjected to a 20 ps rMD run, where the temperature was maintained at 300 K and the force constants were maintained at 20 kcal mol^{-1} Å^{-2} and 80 kcal mol^{-1} rad^{-2} throughout the run. The coordinates were saved at 0.2 ps intervals, and the last 20 coordinates were averaged to obtain a structure that was then subjected to restrained energy minimization to obtain the final structure for that particular duplex (Mujeeb *et al*., 1993).

Assessment of Quality of Structures. The refined structures that resulted from the rMD simulations were evaluated in terms of various energy values, atomic root mean square deviations (rmsd), restraint violations, and the residual indices calculated from the complete relaxation matrix analysis of different intermediate structures. The overall and base pair rmsd values between several starting, intermediate, and final rMD structures were calculated using AMBER 4.1 and are listed in Table 5. The energy terms for various structures were obtained from the output files from energy minimization and rMD calculations and are available as a table in the Supporting Information.

The complete relaxation matrix analysis (CORMA) (Borgias & James, 1988) was used to calculate theoretical two-dimensional NOESY spectra from various starting, intermediate, and final rMD structures. The calculated intensities were compared with the experimental intensities using CORMA to calculate numerical indices that indicate the consistency of the structure with the experimental data using a sixth-root residual index, the dependence of the NOE on the interproton distance. The indices were summed for all the observed intensities, and also as two categories, interresidue and intraresidue cross-peak intensities. In an intraresidue index, both the protons included in the summation must belong to the same residue, while for the interresidue index, the protons do not belong to the same residue. Examination of these indices accentuated structural differences localized in the molecule. A summary of these indices is included in the Supporting Information.

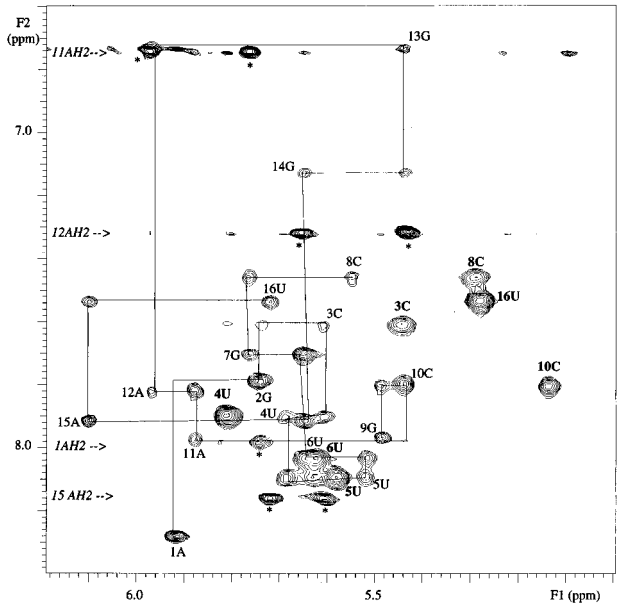

FIGURE 2: Region of the NOESY spectrum containing H8/H6−H1′ cross-peaks for the S2A-C duplex. The spectrum was acquired with a 200 ms mixing time. The intraresidue base proton to H1′ proton cross-peaks are indicated by the residue number, while vertical and horizontal lines show the sequential connectivity. Cross-peaks arising from the H5 to H6 protons of pyrimidines are indicated by bold letters, and cross-peaks from the AH2 to H1′ protons are indicated with asterisks.

Structure Analysis and Display. Sugar pucker and helical parameters were calculated and displayed using the programs CURVES and Dials and Windows (Lavery & Sklenar, 1988; Ravishanker *et al*., 1989). The rmsd values between various structures were calculated using the ANAL module of AMBER 4.1. All structures were displayed and plotted using SYBYL from TRIPOS Inc.

RESULTS

Effects of FUrd on Duplex Stability. The effects of single Urd → FUrd substitutions on the stabilities of oligoribonucleotide duplexes corresponding to region A of stem II of the U4−U6 snRNA complex (Figure 1) were determined both by parametric fitting of individual UV hyperchromicity curves and from the concentration dependence of the T_m. The results are summarized in Table 1. Similar trends for the three duplexes were observed for the two methods. The control duplex S2A-C had a T_m intermediate between those of the two FUrd-substituted duplexes. FUrd substitution at the G-U wobble base pair slightly decreased the T_m, and FUrd substitution at the adjacent A-U base pair slightly increased the T_m. These slight differences in T_m observed for the FUrd-substituted duplexes, relative to the control duplex, were consistent with the calculation of modest differences in the free energy of dissociation for duplexes that differed in FUrd substitution at or near wobble base pairs (Table 1).

NMR Resonance Assignment. The assignments of the nonexchangeable protons for each of the three RNA duplexes (S2A-C, S2A-GF, and S2A-AF) were made in a sequential manner from NOESY and COSY spectra using the strategy

Table 2: Chemical Shifts for Nonexchangeable Protons for the Three Stem II Duplexes

	^{1}H chemical shifts											
	S2A-C				S2A-GF				S2A-AF			
residue	H6/H8	H2/H5	H1′	H2′	H6/H8	H2/H5	H1′	H2′	H6/H8	H2/H5	H1′	H2′
A1	8.28	7.98	5.92	4.68	8.25	7.95	5.90	4.65	8.35	7.85	5.87	4.65
G2	7.79	−	5.74	4.59	7.77	−	5.69	4.60	7.98	−	5.73	4.53
C3	7.62	5.44	5.61	4.57	7.61	5.45	5.58	4.60	7.71	5.38	5.56	4.55
U/F4	7.91	5.81	5.69	4.06	7.99	−	5.63	4.11	7.88	5.79	5.65	4.04
U/F5	8.10	5.58	5.52	4.40	8.13	5.58	5.51	4.43	8.48	−	5.43	4.39
U6	8.03	5.63	5.65	4.57	8.07	5.63	5.67	4.61	8.10	5.66	5.62	4.57
G7	7.71	−	5.76	4.37	7.71	−	5.77	4.40	7.75	−	5.74	4.38
C8	7.46	5.29	5.55	3.94	7.46	5.28	5.53	3.97	7.52	5.33	5.51	3.95
G9	7.97	−	5.49	4.41	7.98	−	5.48	4.43	7.99	−	5.43	4.39
C10	7.80	5.14	5.44	4.55	7.83	5.11	5.42	4.58	7.86	5.10	5.37	4.49
A11	7.98	6.75	5.88	4.48	7.98	6.78	5.88	4.50	8.00	6.77	5.84	4.46
A12	7.83	7.32	5.97	4.49	7.83	7.35	5.97	4.52	7.89	7.36	5.94	4.48
G13	6.74	−	5.44	4.57	6.74	−	5.38	4.58	6.74	−	5.42	4.50
G14	7.13	−	5.65	4.38	7.18	−	5.63	4.42	7.12	−	5.60	4.44
A15	7.92	8.16	6.10	4.39	7.92	8.18	6.10	4.43	7.98	8.27	6.06	4.39
U16	7.54	5.28	5.72	4.02	7.53	5.29	5.69	4.04	7.59	5.25	5.72	4.04

described previously for A-form duplex RNA (Chou *et al*., 1989). Figure 2 shows a portion of the NOESY spectrum for S2A-C in the fingerprint region, illustrating the sequential connectivities in the base H6/H8 to sugar H1′ region. The adenine H2 protons were identified from the characteristic cross-peaks observed with H1′ of the 3′ neighboring residue and with H1′ of the 3′ neighbor of its base pairing partner (Chou *et al*., 1989). The chemical shifts of the nonexchangeable protons (H8/H6, H1′, and H2′) for S2A-C, S2A-GF, and S2A-AF at 15 °C are listed in Table 2. Differences in chemical shift for the base protons and H1′ resonances in the FUrd-substituted sequences compared to the control sequence were limited to the site of substitution.

The exchangeable imino and amino protons for each RNA duplex were assigned using two-dimensional NOESY experiments in H_2O solution (Figure 3). The pathway of sequential connectivity between imino ^{1}H from adjacent base pairs of S2A-C is presented in Figure 3A. The imino protons from the two A-U base pairs (U5 and U6; for numbering, see Figure 1) were assigned to the resonances at 14.1 and 13.2 ppm, respectively, the two most downfield peaks in the ^{1}H spectrum, while the imino protons from G13 and U4 of the G-U base pair were assigned to the resonances at 11.0 and 11.6 ppm, respectively. The intense imino−imino NOE between G13 and U4 is characteristic of wobble geometry for the G-U base pair. The peak at 12.7 ppm was assigned to resonances from two imino protons (G7 and G14) that were degenerate in chemical shift. The imino protons from the terminal base pairs were not detected due to exchange broadening, nor was an imino proton from the putative A-G mismatched base pair observed. NOESY cross-peaks were also observed between the imino and amino ^{1}H resonances of G-C and G-U base pairs, between the uridine imino ^{1}H and AH2 of its base pair partner or its 3′ neighbor, and between the G13 imino ^{1}H and the H1′ of its base pair partner, C3 (Figure 3).

The pathways of sequential connectivity for S2A-GF and S2A-AF are similar to those described for S2A-C and are shown in panels B and C of Figure 3. The NOESY spectra for the FUrd-substituted duplexes differ from those of the control duplex in several properties. First, the FUrd imino ^{1}H for G-FU and A-FU base pairs is broadened and resonates further downfield than does the Urd imino ^{1}H in G-U and A-U base pairs. Similar effects were observed previously for FUrd imino protons from other RNA duplexes (Sahasrabudhe *et al*., 1996). Second, the intensities of both the cross-peaks and the diagonal peaks in two-dimensional NOESY spectra acquired in H_2O solution were greatly diminished for FUrd imino ^{1}H relative to Urd imino ^{1}H for both A-U and G-U base pairs with the exception of the exchange cross-peak of the FUrd imino ^{1}H with H_2O that was increased for the G-FU base pair. The resonance frequencies, line widths, and intensities of cross-peaks and diagonal peaks from other imino ^{1}H, including the partner G for the G-FU base pair, were not affected by FUrd substitution. The chemical shifts for the exchangeable ^{1}H of S2A-C, S2A-GF, and S2A-AF are listed in Table 3.

^{19}F Chemical Shifts. The one-dimensional ^{19}F NMR spectra for S2A-AF and S2A-GF are provided as part of the Supporting Information. The ^{19}F NMR spectrum for each duplex consisted of a single resonance from the site of FUrd substitution. The ^{19}F resonance for S2A-GF, which contains a G-FU base pair, is shifted almost 3 ppm downfield from the ^{19}F resonance from S2A-AF, which contains an A-FU base pair. These results are consistent with previous reports that the ^{19}F signal from base-paired FUra differs considerably between Watson−Crick and wobble geometry (Chu & Horowitz, 1989).

Effects of FUrd on RNA Duplex Structure. The distance and angular constraints applied during the molecular dynamics calculations are summarized in Table 4. The refined structures that resulted from the rMD simulations were evaluated in terms of energy values, restraint violations (Supporting Information), atomic root mean square deviations (rmsd) (Table 5), and the residual indices calculated from the complete relaxation matrix analysis of different intermediate structures (Supporting Information). The values for total energy and constraint violation energy for the final rMD structures were significantly reduced compared to those of the starting structures, indicating compliance of the final structures with the applied experimental constraints. The final, time-averaged structures for S2A-C, S2A-GF, and S2A-AF are presented in Figure 4. Inspection of these structures revealed all three duplexes adopted right-handed, A-form double-helical geometry. Analysis of the helical parameters for each duplex using the program Dials and Windows

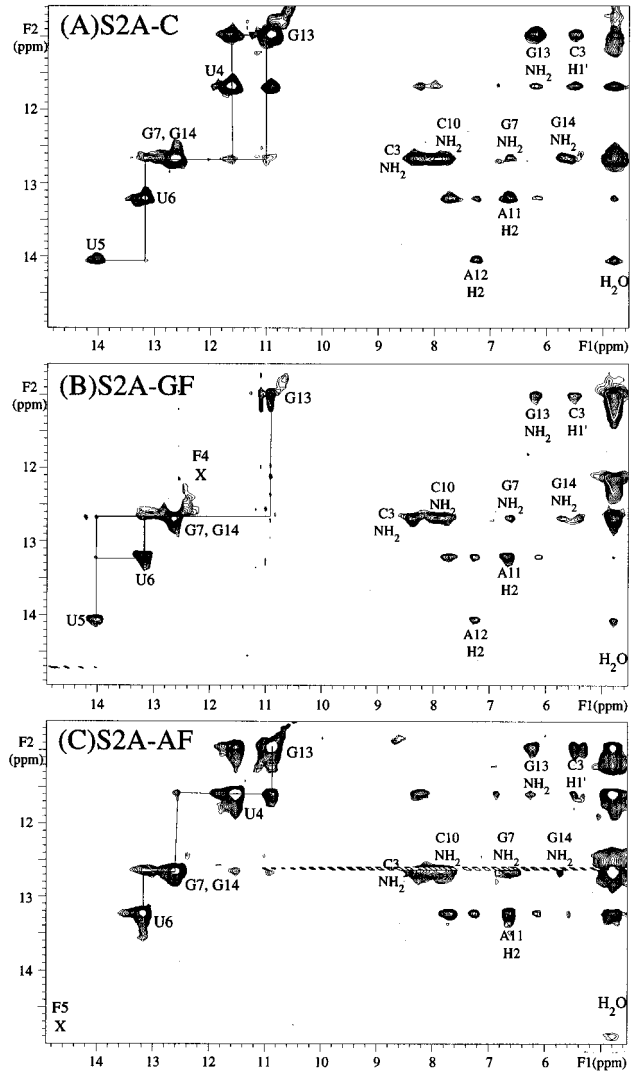

FIGURE 3: Two-dimensional NOESY spectra in H_2O solution showing cross-peaks between the exchangeable imino and amino ^1H resonances. Connectivity between adjacent base pairs is indicated by vertical and horizontal lines. (A) Spectrum for S2A-C. (B) Spectrum for S2A-GF. (C) Spectrum for S2A-AF. Diagonal peaks for the imino ^1H from FUrd in S2A-GF and S2A-AF were not observed due to rapid exchange with solvent and are denoted by an X in parts B and C.

Table 3: Chemical Shifts for the Exchangeable Protons from the Three Stem II Duplexes

	imino proton			amino proton		
residue	S2A-C	S2A-GF	S2A-AF	S2A-C	S2A-GF	S2A-AF
C3	–	–	–	8.29	8.41	8.27
U/F4	11.69	12.16	11.62	–	–	–
U/F5	14.05	14.06	14.91	–	–	–
U6	13.22	13.24	13.24	–	–	–
G7	12.67	12.67	12.60	6.66	6.66	6.66
C10	–	–	–	7.77	7.75	7.75
G13	10.98	11.02	10.99	6.21	6.21	6.23
G14	12.67	12.67	12.60	5.73	5.73	5.78

(Lavery & Sklenar, 1988; Ravishanker *et al*., 1989) confirmed these observations and also established that no systematic differences occurred for the duplexes substituted with FUrd compared to the control duplex. In particular, the helical axis was unchanged in the FUrd-substituted duplexes compared to that of the control duplex. A summary of the analysis obtained using the Dials and Windows software is illustrated in Figure 5.

Table 4: Summary of Applied Constraints during the Restrained Molecular Dynamics Calculations

	S2A-C	S2A-GF	S2A-AF
total number of constraints	301	298	296
distance constraints from NMR	84	81	79
additional indirect constraints[a]	16	16	16
angle constraints from NMR	80	80	80
additional backbone constraints[b]			
distance	13	13	13
angle	74	74	74
hydrogen bond constraints[c]			
distance	17	17	17
angle	17	17	17

[a] Indirect loose constraints in areas poorly defined by NMR constraints (Schmitz *et al*., 1992). [b] These constraints define the right-handedness of the double helix (Baleja *et al*., 1990; Gronenborn & Clore, 1989). [c] These constraints define the Watson−Crick base pairs (Saenger, 1983).

Table 5: (A) Overall[a] and (B) Base Pair rmsd Values for the Three Stem II Duplexes

(A)	final/A-final	final/B-final	A-final/B-final
S2A-C	0.621	1.125	0.563
S2A-GF	0.685	1.199	1.016
S2A-AF	0.558	1.225	1.038

(B) base pair	S2A-C/S2A-GF	S2A-C/S2A-AF
G2-A15	1.456	1.669
C3-G14	0.823	0.529
U/F4-G13	1.490	0.386
U/F5-A12	0.485	1.524
U6-A11	0.788	0.566
G7-C10	0.746	0.685

[a] rmsd between the A-form and B-form starting structures is 4.5 Å.

The overall and base pair rmsd values and energy values for the three duplexes are summarized in parts A and B of Table 5, respectively. The most obvious structural differences in the FUrd-substituted duplexes compared to the control duplex were larger than average base pair rmsds for the base pairs substituted with FUrd (1.5 Å for G-FU or A-FU versus 0.6 Å for other base pairs). Higher than average values of base pair rmsds were also observed for the G-A mismatched base pair in all three duplexes, mainly because of a lack of enough constraints for a more precise definition of the base pair geometry. The G-A mismatched base pair adopted a sheared conformation as was observed previously (Santa Lucia & Turner, 1993; Wu & Turner, 1996). Evidence for the sheared geometry of the G-A base pair includes the absence of any peaks for the G imino proton for the G-A base pair in NOESY spectra and the uniform adoption of sheared geometry for the G-A mismatch for all structures derived from the rMD calculations that were generated without any constraints on hydrogen bonding between the G and the A previously (Santa Lucia & Turner, 1993; Wu & Turner, 1996).

DISCUSSION

The studies reported here provide detailed information on the effects of FUra on the structure and stability of oligoribonucleotide duplexes that correspond to the half of stem II from the human U4−U6 snRNA complex that includes the 5′ terminus of U4 snRNA (Figure 1). This sequence contains an A-G mismatched base pair and a G-U wobble base pair.

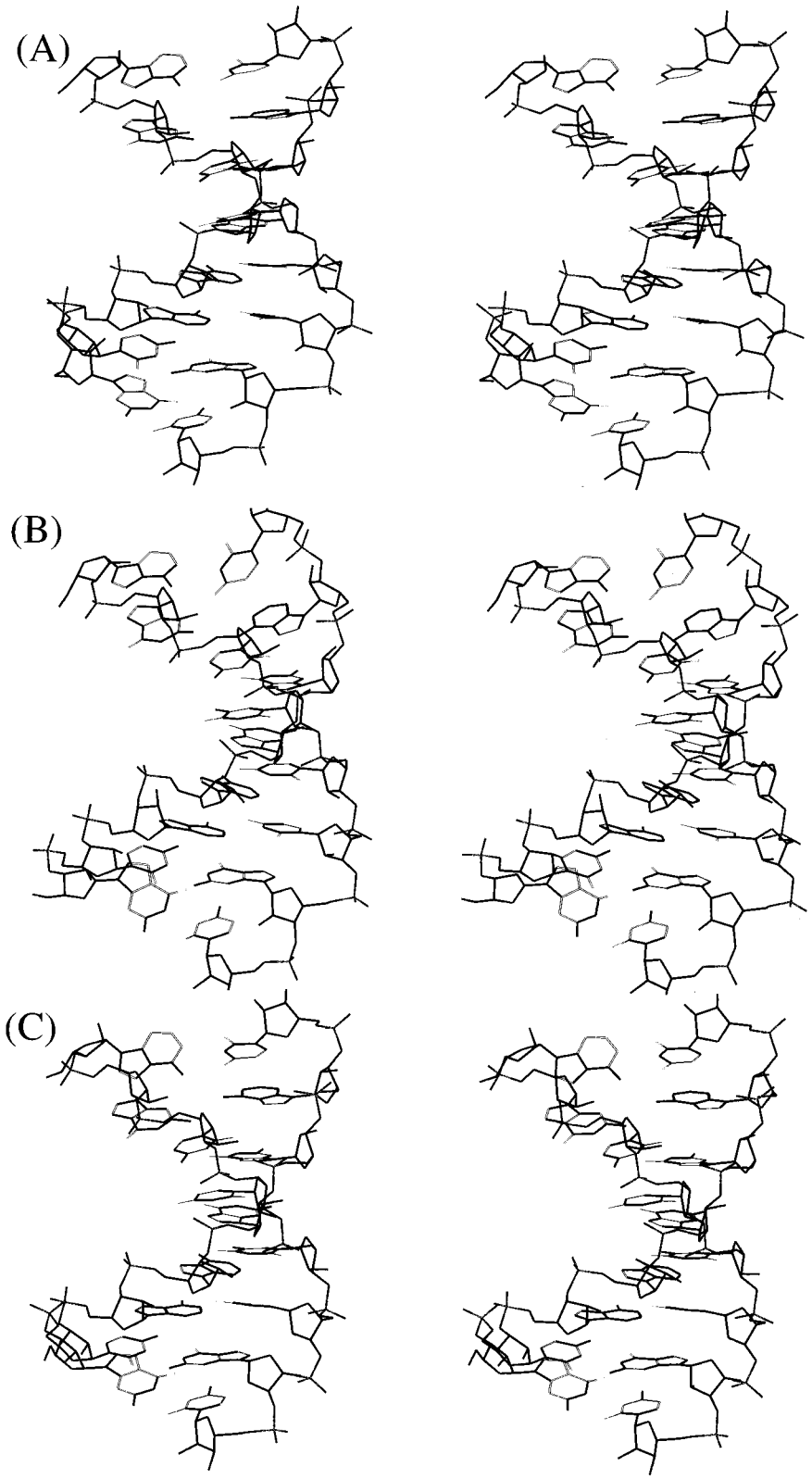

FIGURE 4: Final, time-averaged structures for the three oligoribonucleotide duplexes considered in this study. (A) Structure of the control duplex (S2A-C). (B) Structure of the duplex containing the G-FU base pair (S2A-GF). (C) Structure of the duplex containing the A-FU base pair (S2A-AF). All duplexes adopted A-form helical geometry.

Stem II from the U4−U6 snRNA complex from yeast has been shown to be exquisitely sensitive to mutation, and its stability is critical for the dissociation of this complex that is essential for splicing. The present study documents the fact that the effects of FUrd on the stability of this portion of stem II are modest and unlikely to be significant for the biology of splicing. The effect of FUrd substitution at the G-U wobble base pair was, however, destabilization of the duplex, in contrast to the stabilization that FUrd substitution had been shown to promote in A-U base pairs both in stem II and in other RNA duplexes. The importance of G-U base pairs in RNA biology, including pre-mRNA splicing, raises the possibility that destabilization of select G-U base pairs by FUrd substitution may have deleterious consequences.

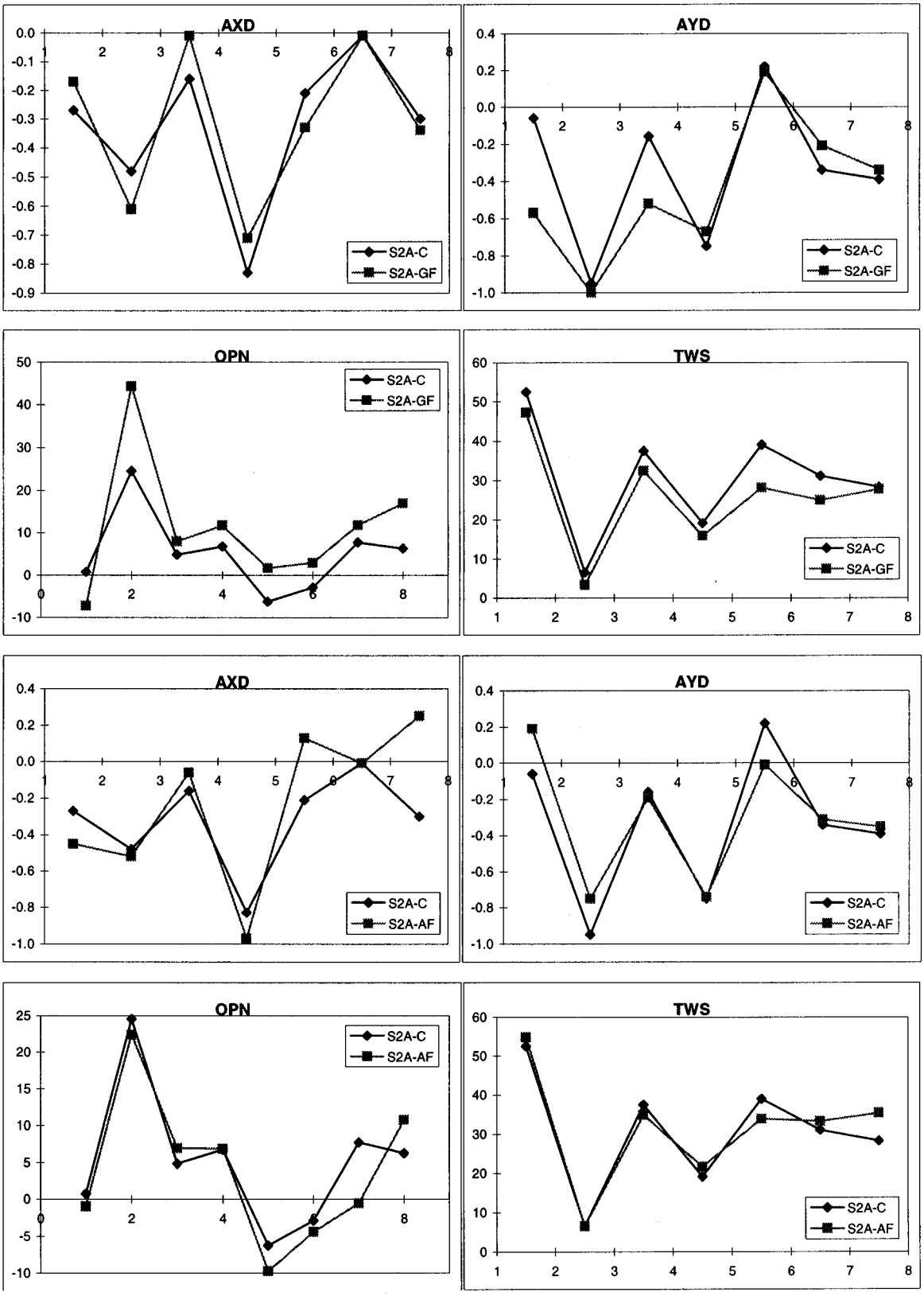

FIGURE 5: Analysis of the helical parameters at each base step for S2A-C, S2A-GF, and S2A-AF.

G-U wobble base pairs occur frequently in RNA and in many cases close the loop region of RNA stem loops (van Knippenberg *et al*., 1990). The propensity of G-U base pairs to close stem loops results from their unique base stacking properties with the G-U base pair stacking much more efficiently with the base pair at the 5′ side of U than with the base pair at the 3′ side of U. In the time-averaged structures shown in Figure 4, G13 and U4 formed a base pair with wobble geometry in S2A-C and S2A-AF. G13 and F4 also formed a base pair with wobble geometry in S2A-GF. U4 (or F4) from the wobble base pair in all three duplexes showed increased stacking with its 5′ neighbor, C3, compared to base pair steps that involved only Watson−Crick base pairs (Figure 6). The corresponding base stacking interaction with U5, the 3′ neighbor of U4 (F4), was significantly reduced (Figure 6), in agreement with previous

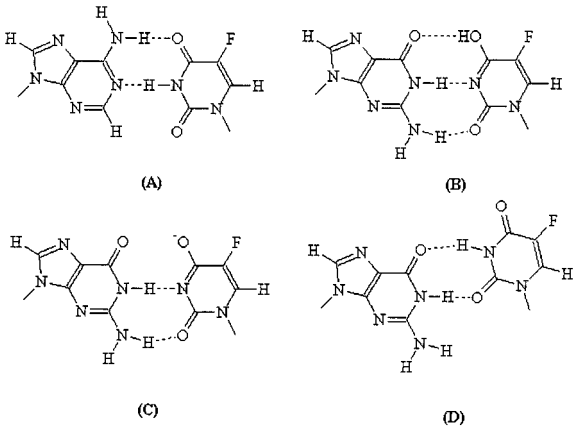

FIGURE 6: Representation of the base overlap that occurs for the G-U base pair of S2A-C and the G-FU base pair of S2A-GF with the 5′ neighboring base pair (relative to U of the wobble base pair) (A) and with the 3′ neighboring base pair (B). Similar representation of base overlap for the A-U base pair of S2A-C and the A-FU base pair of S2A-AF with the 5′ neighboring base pair (relative to U/FU) (C) and with the 5′ neighboring base pair (D). Parts B and C present slightly different views of the same base pair step for S2A-C.

studies of G-U wobble base pair structure (Van Knippenberg *et al*., 1990). The net effect of FUrd substitution in the wobble base pair was increased base stacking between F4 and C3 with little alteration in the stacking geometry between F4 and U5. The increased stacking between F4 and C3 shifted the wobble base pair and reduced stacking between G14 and G13. The destabilization of S2A-GF relative to S2A-C observed in the UV hyperchromicity studies (Table 1) is consistent with the observation of decreased base stacking that occurs between adjacent purines at the base step involving the G-FU wobble base pair in the final, time-averaged structures.

Wobble geometry is one of three plausible geometries for a G-FU base pair in duplex DNA or RNA in which the torsion angles for the glycosidic bonds of both nucleosides are *anti*. Two other reasonable geometries for G-FU base pairs that arise due to the relative acidity of the N3 imino ^{1}H are the enol tautomeric form, with a double bond between N3 and C4 of FUrd, and an ionized base pair, with a formal negative charge at O4 of FUrd (Figure 7). The formation of a dG-FdU base pair having an enol tautomeric form for FdU was discounted by Sowers *et al.* (1988) in their studies of a DNA duplex largely on the basis of the chemical shift for the exchangeable ^{1}H of FdU that resonated at a frequency characteristic of an imino but not an enol ^{1}H. The similarity in the chemical shift of H6 for FdU in dG-FdU and dA-FdU base pairs in their study also was deemed to be inconsistent with tautomerization of FdU since the electronic rearrangement of the pyrimidine ring as a consequence of tautomerization would be expected to strongly impact the H6 chemical shift. The adoption of an enol tautomeric form for the G-FU base pair in S2A-GF in the present study can be discounted on the basis of these same arguments.

Sowers and co-workers also observed pH-dependent changes in the chemical shifts for H6 and F5 of FdU for a DNA duplex that contained a dG-FdU base pair and concluded that a pH-dependent equilibrium between wobble and ionized base pair geometry occurred for the dG-FdU base pair in the DNA duplex with wobble geometry favored by a 9/1 ratio near physiological pH. The observation of pH-dependent changes in chemical shift does not prove, however, that the ionized form of FdU occurred base-paired and in the interior of the helix. Reports of FdU-dG base pairs in duplex DNA (Coll *et al*., 1989) and FU-G base pairs in tRNA (Chu & Horowitz, 1989) have revealed no evidence for formation of ionized base pairs. Evidence from the present study clearly indicates that the FUrd imino ^{1}H exchanges rapidly with H_2O. This rapid exchange results in greatly diminished intensities for the diagonal peaks and cross-peaks in the two-dimensional NOESY spectra acquired in H_2O solution with the exception of the exchange cross-peak with H_2O (Figure 3). These data are, however, inconsistent with formation of an ionized base pair (Figure 7C) in two respects. First, the chemical shifts for the G NH and NH_2 ^{1}H are the same for the G-U and G-FU base pairs in S2A-C and S2A-GF. An ionized base pair would be expected to perturb the electronic environment and affect the chemical shifts for ^{1}H near the localization of charge. Second, the NOE intensity between G NH and NH_2 ^{1}H is similar for G-U and G-FU base pairs. While this interproton distance is constrained by chemical bonds to be nearly identical for ionized and wobble base pairs, hydrogen bond formation for G NH_2 in the ionized base pair would restrict rotation about the C−N bond and result in a strong NOE between the hydrogen-bonded imino and amino ^{1}H for G in the G-FU ionized base pair. In fact, the NH−NH_2 cross-peak in the two-dimensional NOESY spectrum in H_2O solution for the G-FU base pair is slightly weaker than for the G-U base pair and is significantly weaker than for the imino−imino NOESY cross-peak for the G-U wobble base pair in S2A-C.

The effect of FUrd substitution at both G-U and A-U base pairs in duplex RNA is mainly on the dynamics of base pair opening and exchange (Leroy *et al*., 1988). Increased chemical exchange of the FUrd imino ^{1}H with solvent H_2O is evident in the two-dimensional NOESY spectra acquired in H_2O solution (Figure 3). Imino ^{1}H exchange for FUrd, in contrast to Urd, is not base catalyzed near physiological pH (W. H. Gmeiner, unpublished data), and the exchange rates for FUrd imino ^{1}H are much faster than those for Urd. While the chemical shift and NOESY intensity data argue against formation of an ionized G-FU base pair, all of the experimental evidence is consistent with FUrd adopting an extrahelical conformation that is partially ionized and that is in equilibrium with a base pair having wobble geometry. Hydrogen exchange occurs only when the nucleoside base is extrahelical and is elevated for FUrd relative to Urd because of the electron-withdrawing effect of F5. Both the A-FU and G-FU base pairs of S2A-AF and S2A-GF showed greater rmsd values than did other base pairs in this study. This increased rmsd reflects greater uncertainty in the position of these base pairs as would occur if an extrahelical component was providing a greater contribution to the time-averaged structure of these RNA duplexes. This model is also consistent with ^{19}F NMR data from the present study. The difference in chemical shift for the ^{19}F resonance of S2A-GF compared to that of S2A-AF was 2.6 ppm, somewhat less than the 4.5 ppm downfield shifts observed previously upon A-FU Watson−Crick to G-FU wobble base pair transitions in tRNA (Chu & Horowitz, 1989). The reduced difference in chemical shift for ^{19}F in S2A-GF relative to that in S2A-AF compared to chemical shift differences resulting from similar substitutions in tRNA may be a

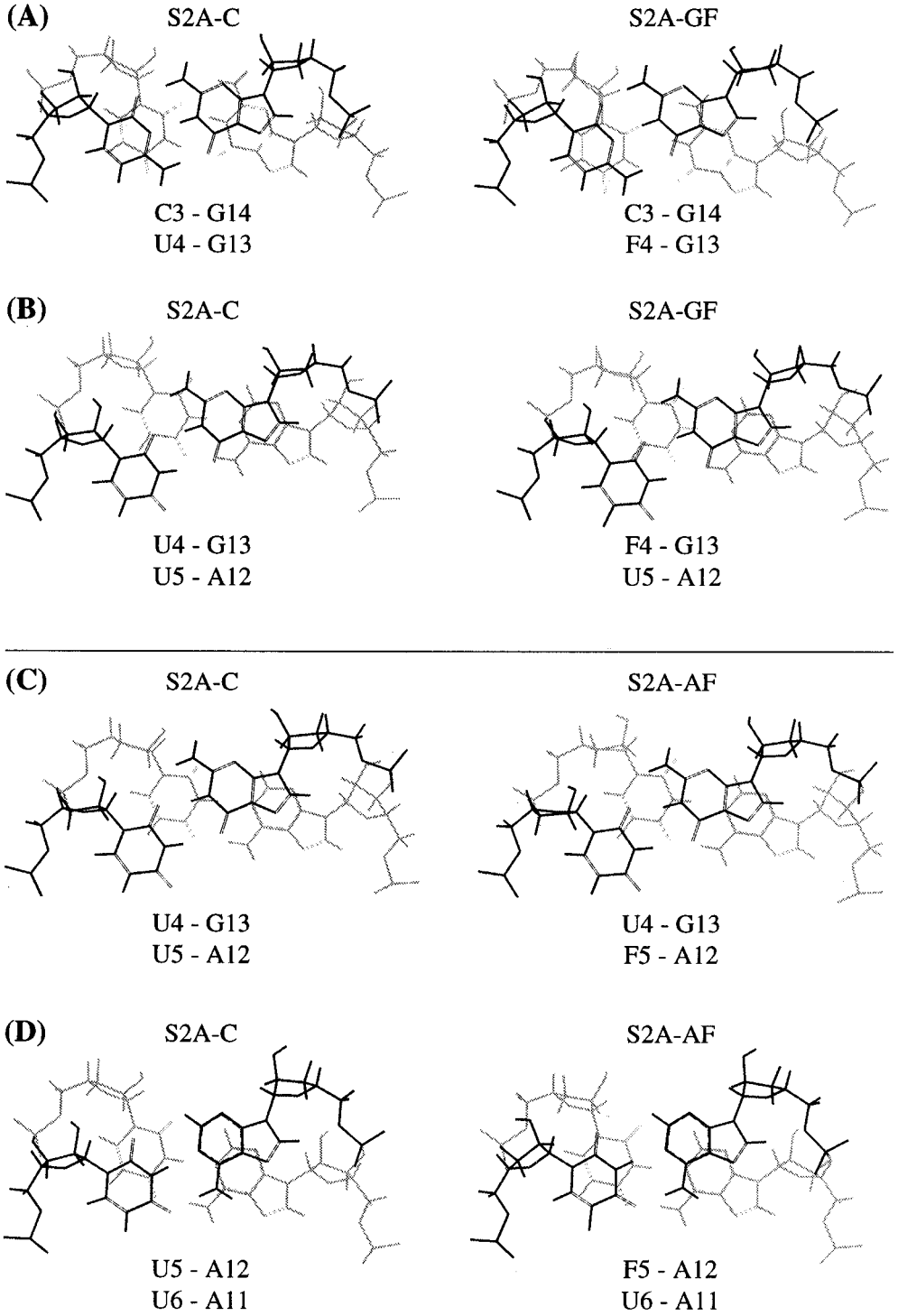

FIGURE 7: Possible geometries for the G-FU base pair for S2A-GF. (A) Normal Watson−Crick base pair between FU and A. (B) The enol tautomeric form of FU base paired with G. (C) Ionized FU base paired with G. (D) The G-FU wobble base pair that occurs in S2A-GF.

consequence of greater dynamic motion in these low-melting duplexes compared to the more rigid structure of tRNA. Fluctuations in the periodicity of extrahelical motion, rather than changes in time-averaged structure, may be the basis for the deleterious effects of FUra on nucleic acid function.

RNA-mediated processes are critical for the function of all living cells. Although it was recognized shortly after initial observations of 5-FU cytotoxicity that substitution of uridine by 5-fluorouridine in cellular RNA could be responsible, in part, for the anticancer activity of this drug, few data directly assessing the effects of Urd → FUrd substitution on RNA structure and function have become available (Chaudhuri *et al.*, 1958). The present study documents the effects of Urd → FUrd substitution in a model duplex derived from the stem II region of the U4−U6 snRNA complex. FUrd substitution had only a minor effect on the structure and stability of this model duplex. Although we cannot eliminate the possibility that the effects of Urd → FUrd substitution on the stability and structure of the U4−U6 snRNA complex *in vivo* may be larger or more significant than the effects observed in this model duplex, the data indicate that Urd → FUrd substitution at G-U wobble base pairs in RNA duplexes is unlikely to affect the structure or function of RNA. RNA-mediated effects of 5-FU probably

arise from Urd → FUrd substitution in nonduplex regions of RNA or from disruption of RNA−protein recognition processes.

ACKNOWLEDGMENT

The authors thank Dr. Jack Horowitz for critical reading of the manuscript.

SUPPORTING INFORMATION AVAILABLE

^{19}F NMR spectra for S2A-GF and S2A-AF, tables listing the energy terms for the starting and final structures, and an analysis of the fit between the calculated and experimental NOE intensities for the starting and final structures (3 pages). Ordering information is given on any current masthead page.

REFERENCES

Arnott, S., & Hukins, D. W. L. (1972) *Biochem. Biophys. Res. Commun. 47*, 1504−1509.
Arnott, S., & Hukins, D. W. L. (1973) *J. Mol. Biol. 81*, 93−105.
Babcook, D. M., Sahasrabudhe, P. V., & Gmeiner, W. H. (1996) *Magn. Reson. Chem. 34*, 851−857.
Baleja, J. D., Pon, R. T., & Sykes, B. D. (1990) *Biochemistry 29*, 4828−4839.
Borer, P. N., Dengler, B., Tinoco, I., Jr., & Uhlenbeck, O. C. (1974) *J. Mol. Biol. 86*, 843−853.
Borgias, B. A., & James, T. L. (1988) *J. Magn. Reson. 79*, 493−512.
Borgias, B. A., & James, T. L. (1989) Two-dimensional nuclear Overhauser effect: complete relaxation matrix analysis, in *Nuclear Magnetic Resonance, Part A: Spectral Techniques and Dynamics* (Oppenheimer, N. J., & James, T. L., Eds.) Academic Press, New York.
Borgias, B. A., & James, T. L. (1990) *J. Magn. Reson. 87*, 475−487.
Chaudhuri, N. K., Montag, B. J., & Heidelberger, C. (1958) *Cancer Res. 18*, 318−328.
Cheng, Y., & Nakayama, K. (1983) *Mol. Pharmacol. 23*, 171−174.
Chou, S.-H., Flynn, P., & Reid, B. (1989) *Biochemistry 28*, 2422−2435.
Chou, S.-H., Cheng, J. W., & Reid, B. R. (1992) *J. Mol. Biol. 228*, 138−155.
Coll, M., Saal, D., Fredrick, C. A., Aymami, J., Rich, A., & Wang, A. H.-J. (1989) *Nucleic Acids Res. 17*, 911−923.
Daher, G. C., Harris, B. E., & Diasio, R. B. (1990) *Pharmacol. Ther. 48*, 189−222.
Doong, S.-L., & Dolnick, B. J. (1988) *J. Biol. Chem. 263*, 4467−4473.
Gmeiner, W. H., Anderson, J., & Sahasrabudhe, P. (1994a) *Nucleosides Nucleotides 13*, 2329−2344.
Gmeiner, W. H., Sahasrabudhe, P. V., & Pon, R. T. (1994b) *J. Org. Chem. 59*, 5779−5783.
Gronenborn, A. M., & Clore, G. M. (1989) *Biochemistry 28*, 5978−5984.
Harris, D. R., & Macintyre, W. M. (1964) *Biophys. J. 4*, 203−225.
Hore, P. J. (1983) *J. Magn. Reson. 55*, 283−300.
Houghton, J. A., Harwood, F. G., & Houghton, P. J. (1994) *Cancer Res. 54*, 4967−4973.
Hu, J., Xu, D., Schappert, K., Xu, Y. J., & Friesen, J. D. (1995) *Mol. Cell. Biol. 15*, 1274−1285.
Ingraham, H. A., Tseng, B. Y., & Goulian, M. (1980) *Cancer Res. 40*, 998−1001.
Lavery, R., & Sklenar, H. (1988) *J. Biomol. Struct. Dyn. 6*, 63−91.
Leroy, J. L., Kochoyan, M., Huynh-Dinh, T., & Gueron, M. (1988) *J. Mol. Biol. 200*, 223−228.
Mujeeb, A., Kerwin, S. M., Kenyon, G. L., & James, T. L. (1993) *Biochemistry 32*, 13419−13431.
Parker, W. B., & Cheng, Y. C. (1990) *Pharmacol. Ther. 48*, 381−395.
Pearlman, D. A., Case, D. A., Caldwell, J. W., Ross, W. S., Cheatham, T. E., III, Ferguson, D. M., Seibel, G. L., Singh, U. C., Weiner, P., & Kollman, P. (1995) *AMBER 4.1*.
Petersheim, M., & Turner, D. H. (1983) *Biochemistry 22*, 256−263.
Pratt, W. B., Ruddon, R. W., Ensminger, W. D., & Maybaum, J. (1994) *The Anticancer Drugs*, Oxford University Press, New York.
Ravishanker, G., Swaminathan, S., Beveridge, D. L., Lavery, R., & Sklenar, H. (1989) *J. Biomol. Struct. Dyn. 6*, 669−699.
Ryckaert, J. P., Cicotti, G., & Berendsen, H. J. C. (1977) *J. Comput. Phys. 23*, 327−341.
Saenger, W. (1984) *Principles of Nucleic Acid Structure*, Springer-Verlag, New York.
Sahasrabudhe, P. V., Pon, R. T., & Gmeiner, W. H. (1995) *Nucleic Acids Res. 23*, 3916−3921.
Sahasrabudhe, P. V., Pon, R. T., & Gmeiner, W. H. (1996) *Biochemistry 35*, 13597−13608.
Santa Lucia, J., Jr., & Turner, D. H. (1993) *Biochemistry 32*, 12612−12623.
Santi, D. V., McHenry, C. S., & Sommer, H. (1974) *Biochemistry 13*, 471−480.
Schmitz, U., Sethson, I., Egan, W., & James, T. L. (1992) *J. Mol. Biol. 227*, 510−531.
Schuetz, J. D., Collins, J. M., Wallace, H. J., & Diasio, R. B. (1986) *Cancer Res. 46*, 119−123.
Scmittgen, T. D., Danenberg, K. D., Horikoshi, T., Lenz, H.-J., & Danenberg, P. V. (1994) *J. Biol. Chem. 269*, 16269−16275.
Singh, U. C., Weiner, S. J., & Kollman, P. (1985) *Proc. Natl. Acad. Sci. U.S.A. 82*, 755−759.
Sowers, L. C., Eritja, R., Kaplan, B., Goodman, M. F., & Fazakerley, G. V. (1988) *J. Biol. Chem. 263*, 14794−14801.
Spiegelman, S., Nayak, R., Sawyer, R., Stolfi, R., & Martin, D. (1980) *Cancer 45*, 1129−1134.
States, D. J., Haberkorn, R. A., & Ruben, D. J. (1982) *J. Magn. Reson. 48*, 286−292.
Stolarski, R., Egan, W., & James, T. L. (1992) *Biochemistry 31*, 7027−7042.
Suzuki, E., Pattabiraman, N., Zon, G., & James, T. L. (1986) *Biochemistry 25*, 6854−6865.
Tanaka, M., Yoshida, S., Saneyoshi, M., & Yamaguchi, T. (1981) *Cancer Res. 41*, 4132−4135.
Van Knippenberg, P. H., Formenoy, L. J., & Heus, H. A. (1990) *Biochim. Biophys. Acta 1050*, 14−17.
Weckbecker, G. (1991) *Pharmacol. Ther. 50*, 367−424.
Wilkinson, D. S., & Pitot, H. C. (1973) *J. Biol. Chem. 248*, 63−68.
Wu, M., & Turner, D. H. (1996) *Biochemistry 35*, 9677−9689.

BI9700577